Plasmon-Induced Simultaneous Electrochemical and Fluorescence Switches Probed by Combined SECM and Fluorescence Microscopy

Ali Dabbous, Baptiste Maillot, Jean-Frédéric Audibert, Vitor Brasiliense, Fabien Miomandre

Plasmon-Induced Simultaneous Electrochemical and Fluorescence Switches Probed by Combined SECM and Fluorescence Microscopy

Ali Dabbous, Baptiste Maillot, Jean-Frédéric Audibert, Vitor Brasiliense, and Fabien Miomandre*

ABSTRACT: An unprecedented dual simultaneous switch of fluorescence intensity and electrochemical current induced by plasmon activation is demonstrated using a combination of electrochemical (SECM) and fluorescence microscopies with a fluorescent redox-active probe (tetrazine derivative) in solution. The mechanism of this dual switch is assigned to an asymmetric charge injection involving holes rather than electrons, despite the oxidant character of the redox probe. Thermal effects due to plasmon activation have been measured by using quantitative phase imaging and revealed negligible solution temperature increases, corroborating the main role of charge injection. This demonstrates for the first time that electrofluorochromism, which involves a redox switch monitoring the luminescence properties, can be optically triggered.

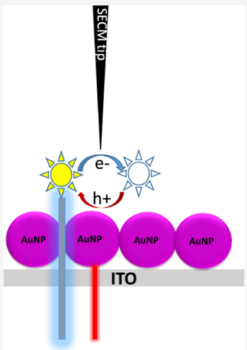

INTRODUCTION

Plasmon-mediated (or plasmon-driven) electrochemistry has become a field of great interest in the past decade, as highlighted by recent reviews of the field.[1,2] When plasmonic nanostructures are illuminated with light at their resonance wavelength, they generate hot carriers, which can be used to carry out redox transformations.[3] This concept finds valuable applications in the framework of electrocatalysis[4,5] and photoelectrochemical devices[6,7] as visible light[6] can be efficiently used to induce electrochemical reactions, in contrast to the UV light usually required with semiconducting electrode materials. This was recently applied on several electrochemical reactions of broad interest like hydrogen evolution[8] or methanol oxidation.[9] The electrochemical process can be coupled with light emission, like electrochemiluminescence, opening the route toward detection at the microscopic level and even down to the single particle level,[10] with direct applications in biosensors with enhanced sensitivity.[11,12]

Plasmon activation can also directly impact light emission properties either by quenching or enhancing the emission intensity depending on the experimental conditions.[13−15] In most cases, the mechanism relies on energy transfer between the plasmonic structure and the luminophore. When emitted light is in resonance with plasmon excitation, energy transfer results in efficient quenching, whereas the opposite occurs if the excitation wavelength matches the plasmon resonance, leading to local enhancement of the electromagnetic field.

Beyond these phenomena, as plasmon excitation results in charge carrier injections able to drive an electrochemical reaction, itself likely to control emission like in electrofluorochromic molecules[16] and materials,[17] one comes to the conclusion that a remote control of emission by plasmon excitation should be possible based on charge carrier injection in solution. In such a case, a dual control can be operated on light emission based on either the electrochemical reaction alone classically triggered by the electrode potential or an optical signal inducing this electrochemical reaction by the plasmon-driven charge injection. This creates a new pathway in plasmon-mediated light emission through a redox switch. An additional interest here concerns the analysis of the mechanism involved in this phenomenon. When dealing with plasmon-assisted electrochemistry, many studies focused on the Au−TiO_2 interface targeting water photodissociation.[7] The main issue is to disentangle the charge carrier injection process from side-effects, one among which is temperature enhancement.[18−20] Using an electrofluorochromic compound as the redox probe allows one to dispose of two output signals to report the effects of plasmonic activation, among which the emission can be used to image the spatial extent of the phenomenon. To achieve that experimentally, we chose a configuration in which the electrochemical signal can be applied at a different location from the plasmonic substrate in order to ensure that both input signals are applied independently. This can be done by combining fluorescence microscopy with scanning electrochemical microscopy (SECM).[21,22] The use of SECM to report plasmon-activated

Scheme 1. Experimental Setup Coupling Electrochemical Microscopy (SECM, Green Upper Part), Epifluorescence Microscopy with a Dual Excitation Pathway (Yellow Lower Part), and Quantitative Phase Microscopy for Phase Imaging (Orange Lower Left Part)

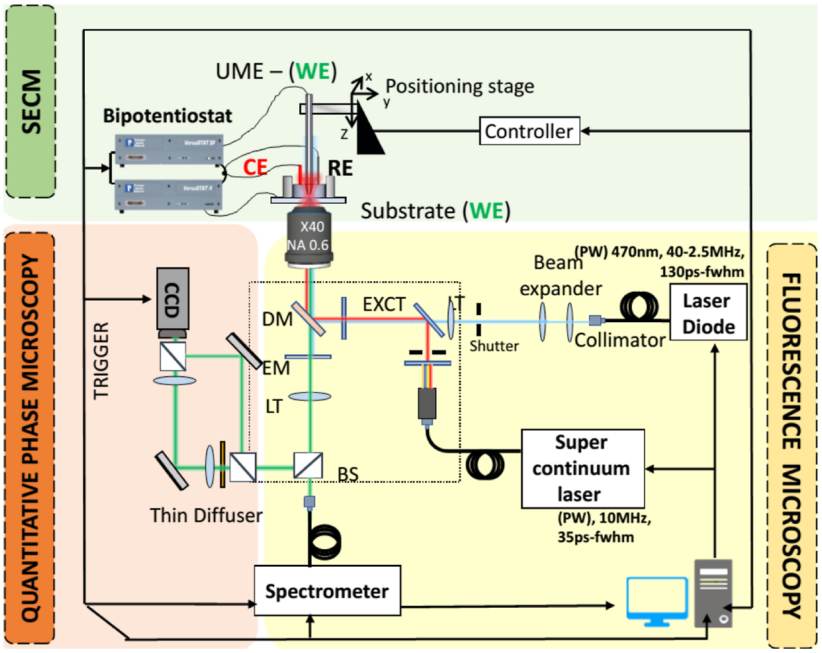

electrochemical reactions occurring on a substrate was initially reported by Willets et al.[18] in aqueous solutions with pure redox probes. Furthermore, the topic has been highlighted recently[23] with mechanisms claimed to be based on photothermal enhancement of mass transport.[24,25] If hole/electron injection is thought to be a competitive process, then a great advantage of this configuration is a direct report of the type of charge carrier likely to be injected in solution to perform the electrofluorochromic reaction. Indeed, imposing the electrochemical reaction at the tip, the measured current is sensitive to the electrochemical reaction occurring on the substrate in a simple way: current enhancement if the substrate reaction is opposite to the tip reaction (positive feedback) and current decrease in the opposite case (negative feedback). This paper thus reports the first example of plasmon-driven electrochemistry reported by a combination of SECM and fluorescence microscopy with an electrofluorochromic probe in solution, namely, 1-chloro-4-ethoxy-*s*-tetrazine (ClTzOEt). Tetrazines are good candidates as they emit in the visible range under visible excitation and are easily reducible compounds with reversible electrochemistry.[26,27] We will show here that the main reaction observed upon plasmonic activation is hole injection, although the redox probe cannot be directly oxidized. Fluorescence quenching induced either electrochemically or by plasmon activation is observed, and the involved mechanism is thoroughly investigated.

■ EXPERIMENTAL SECTION

All commercial chemicals were used as received without further purification.

Plasmonic Substrates. The plasmonic substrates on ITO were electrochemically prepared on 25 mm × 25 mm ITO plates (25−35) Ω cm, 100 nm thickness from SOLEMS SAS (France) by chronoamperometry using a HTDS VersaSTAT 3 potentiostat, according to a previously published protocol.[28] A three-electrode setup with the ITO plate as the working electrode, a silver wire as a quasi-reference electrode (QRE), and a platinum wire as the counter electrode was used for electrochemical experiments. The electrolyte solution was prepared from chloroauric acid trihydrate (from Sigma-Aldrich >99.9%) (2 mM) and sodium carbonate (from Prolabo 0.25M) in milli-Q water (18.2 MΩ cm^{-1}). The electrodepositions were carried out at constant potential fixed at −0.6 V, −0.7 V, −0.8 V, −0.9 V, −1 V, and −1.1 V vs Ag QRE for 300 s.

The plasmonic substrates on glass were prepared according to an optimization of a reported procedure.[18] Briefly, it consisted of evaporating gold metal (99.95%, Ted Pella, Inc.) on glass coverslips (Fisher Scientific) using an evaporator (Nano 36, Lesker). Then the substrates were heated using the COMO ceramic oven at 250 °C for 4 h, resulting in plasmonic substrates with a plasmon resonance band close to 650 nm.

Absorption spectra of a plasmonic substrate are shown in Figure S1 at various locations under microscope for transmitted light detection, to check the good homogeneity of the response.

Absorption Spectroscopy. Extinction spectra of the nanoparticles were recorded by using a SD 2000 fiber optic spectrometer from Ocean Optics. The samples were illuminated in transmission mode using a Nikon inverted microscope with a 12 V 100 W halogen lamp through a 40× objective (NA 0.6). Spectra were acquired using the SpectraSuite software in absorbance mode with an integration time of 1 s. The presented spectra are averages of 100 raw spectra corrected for the dark signal.

Electrochemistry. Electrochemistry experiments were performed with a HTDS VersaSTAT 3F potentiostat. A three-electrode setup with a 10 μm Pt ultramicroelectrode (from HTDS) as the working electrode, a silver wire as a QRE, and a platinum wire as the counter electrode was used. In the four-electrode mode, substrates were polarized using a HTDS VersaSTAT 4 potentiostat, which shared the same reference

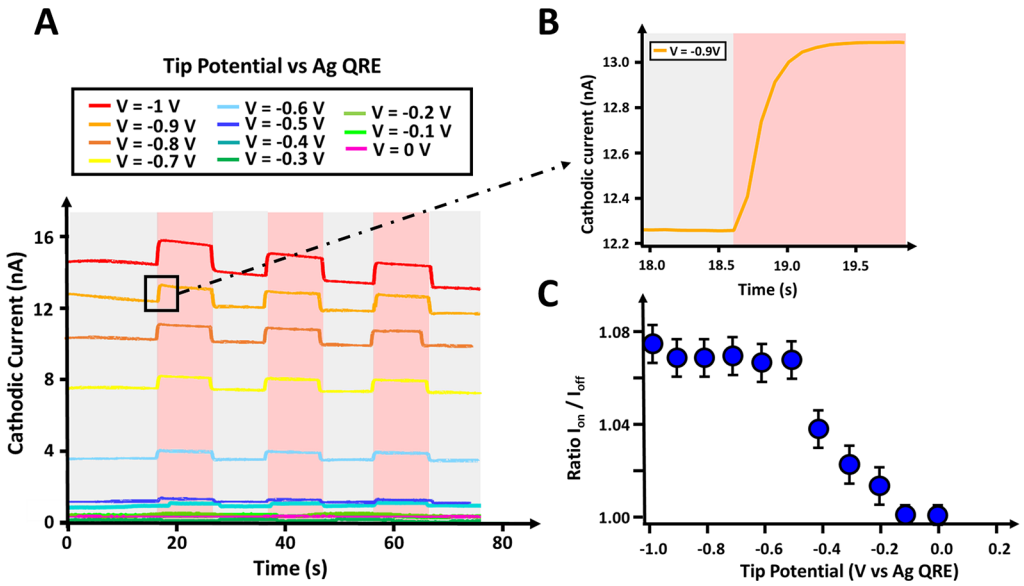

Figure 1. A) Electrochemical current vs time for steps from 0 to various tip potentials. Red zones correspond to plasmon activation (650 nm laser switch on). (B) Raising part of the current for the first step of the orange trace in (A). (C) Variation of the current contrast ratio between the ON (plasmon activation) and OFF (no plasmon activation) states as a function of the tip potential. Tip−substrate distance = 10 μm.

and counter wires as the VersaSTAT 3F. The tip position was controlled by a piezoelectric system (VersaSCAN). Plasmonic substrates were illuminated using a supercontinuum laser (SMHP-40.2- A-PP-RC, Leukos 10 MHz−40 ps-fwhm). The excitation wavelength was selected by using a bandpass filter (BP650 nm-13 nm from Semrock).

For all experiments, the electrolyte solution was prepared by dissolving 1-chloro-4-ethoxy-(2,3,5,6)-tetrazine (ClTzOEt, synthesized in the lab according to a reported protocole[29]) 2 mM and tetrabutylammonium hexafluorophosphate (from TCI > 98%) 0.1 M either in acetonitrile (from Carlo Erba Reagents) or a mix (9:1) of absolute anhydrous ethanol (from Carlo Erba Reagents) and acetonitrile.

Fluorescence Microscopy Coupled to SECM. The optical measurements were carried out on a Nikon Ti Eclipse inverted microscope with an extra-large working distance objective (40×, NA 0.6) in wide-field illumination (see Scheme 1). In the last part, confocal configuration with a (×100, NA 1.49) objective was used.

Tetrazine molecules were excited by a pulsed laser diode at 474 nm (LDH−P−C−470B, PicoQuant) with pulses of 230 ps and a repetition rate of 40 MHz with a power density of ca. 30 W cm^{-2}. The plasmonic substrates were excited by using a supercontinuum laser (SMHP-40.2−A-PP-RC, Leukos 10 MHz−40 ps-fwhm) with a band-pass filter (BP650 nm-13 nm from Semrock) with a power of 650 μW focused in a 20 μm diameter zone (power density of ca. 20 kW cm^{-2}). The emitted light was collected after passing through a band-pass filter (BP536 nm-40 nm from Semrock).

Electrofluorochromism was studied by recording the emitted light during multistep chronoamperometry experiments. The emitted light was collected on a CCD camera (PixelFly USB CCD, from PCO AG) with an integration time of 300 ms during multistep chronoamperometry.

Quantitative Phase Imaging. Quantitative phase imaging (QPI) experiments were conducted using a DiPSI module to the detection pathway (see Scheme 1), as described in detail elsewhere.[30] Briefly, we used a 4f setup to position a thin diffuser a few millimeters (3 mm) away from the plane conjugated to the CCD sensor. This generates a random interference (speckle) pattern whose deformation can be associated with local phase gradients, which by integration reveals the optical path difference (OPD) with respect to a reference. In addition to the microscope objective (×40, NA = 0.6), we used a ×1.5 tube lens and a ×2.5 relay lens to achieve a ×150 total magnification. In these experiments, the microscope native source in the Köhler configuration is equipped with a filter (λ_{obs} = 536 nm, 40 nm fwhm) to avoid plasmon excitation, leading to an average power density of 500 mW cm^{-2}. Illumination NA is kept below 0.2 to ensure spatial coherency of the illumination. The plasmon excitation wavelength is eliminated with the help of a bandpass 543 nm, 22 nm-fwhm filter (Multiband dichroic TFT503/582/658(HE) from Zeiss). The speckle images were processed with the help of MATLAB, implementing the image registration routines as described in the literature,[31] leading to the images shown in the paper.

The overall experimental setup is shown in Scheme 1.

RESULTS AND DISCUSSION

Simultaneous electrochemical and optical detections were performed by using the dual excitation pathways likely to activate plasmons of the gold nanoparticles along with the emission of the fluorophores. The results are discussed below by considering first the electrochemical response and then fluorescence detection. Finally, QPI was implemented to evaluate the thermal contribution associated with plasmon activation.

Electrochemical Response. A first set of data has been collected by using the SECM tip to measure electrochemical current under plasmon activation of Au NPs on ITO (laser power 650 μW, focal point 4 μm diameter) in a configuration similar to the one used by Willets et al.[18] First, the plasmonic substrate is kept in open circuit, while the tip is polarized at 0 V for a few seconds and then at various potentials, inducing the tetrazine (Tz) reduction into its anion radical (see CV in Figure S2). We thus sequentially probe the current associated

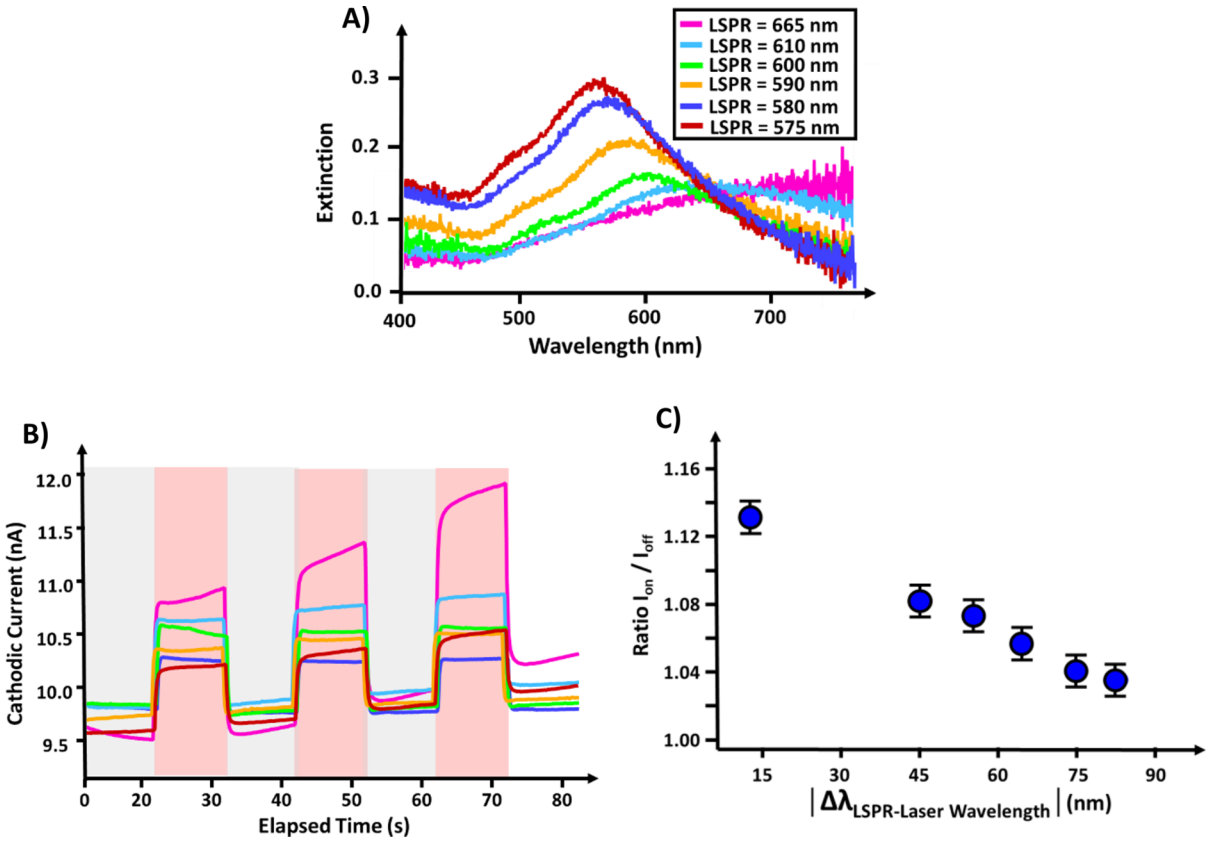

Figure 2. (A) Extinction spectra of the various nanoparticle arrays deposited on ITO as a function of the electrodeposition potential. (B) Electrochemical current vs time for three successive ON−OFF states induced by polarizing the tip at −0.9 V. Plasmon activation (red laser on, 650 μW) in the red zones. (C) Intensity contrast ratio vs the difference between laser excitation and maximum plasmon resonance wavelength. Tip−substrate distance = 10 μm.

with Tz reduction in the absence (red laser OFF) and presence (red laser ON) of plasmonic excitation. When the red laser is switched on, a clear enhancement of the electrochemical current is observed (Figure 1A, red zones) and the current goes back to its initial value as soon as the red irradiation stops (gray zones). A closer look at the raising part of the current step demonstrates that the limiting value is reached in ca. 0.5 s (Figure 1B), a time range that is fully consistent with a diffusion process in the 10 μm tip−substrate distance.

The phenomenon can be quantified by reporting the ratio between the tip current in the absence and presence of plasmon excitation ($r = i_{ON}^{tip}/i_{OFF}^{tip}$; see Supporting Information for details on how it is determined), hereafter called the contrast current ratio. As shown in Figure 1C, when the tip potential is not negative enough to allow the tetrazine reduction, no change in the current can be seen upon plasmon activation, and the contrast ratio is equal to 1. This demonstrates that a direct plasmon-driven reduction of tetrazine can be excluded since it should have an impact on the feedback current measured at the tip. This is a first noticeable result, having in mind that tetrazines are quite good electron acceptors, attested by their relatively high reduction potential for a small aromatic molecule. Then, as soon as the tip potential becomes more negative than the half-wave potential of the redox probe, the ratio tends toward a limiting value, which is in our case around 1.07. These results are consistent with a positive feedback occurring upon plasmon activation on the substrate, that is hole injection allowing the oxidation of the anion radical produced at the tip and diffusing toward the substrate, thus regenerating the probe in its oxidized state. Note that the curve of Figure 1C is very similar to the CV of the redox probe (Figure S2), with a half-wave potential positively shifted by about 100 mV.

To check the mechanism involved in this plasmon enhanced electrochemical current, several control experiments were performed. The first one concerns the influence of the tip−substrate distance. In a such a feedback mode, the electrochemical current is expected to be strongly dependent on the tip−substrate distance, and this is indeed the case (Figure S3). When the distance is larger than 100 μm, i.e., 10 times the tip radius, no variation of the tip current is observed under plasmon excitation, whereas a quasi-linear variation of the contrast ratio can be seen with the logarithm of the distance in the range (10−100 μm), i.e., between one and ten times the tip radius. The maximum value of r is obtained when the distance is within the order of magnitude of the tip radius.

We also confirmed the previous observations by noticing that the contrast ratio was also sensitive to the alignment between the tip and the illuminated region (focal point of red irradiation). When the tip position is shifted horizontally vs this point, the contrast ratio becomes quickly much smaller (Figure S4). Finally, it is observed that the contrast ratio depends linearly on the red light excitation power (Figure S5) and thus apparently scales with the number of injected charge carriers. Indeed, if thermal effects were responsible for the current enhancement, they should not vary linearly with the laser power because the electrochemical current depends on the square root of the diffusion coefficient, which in turn varies

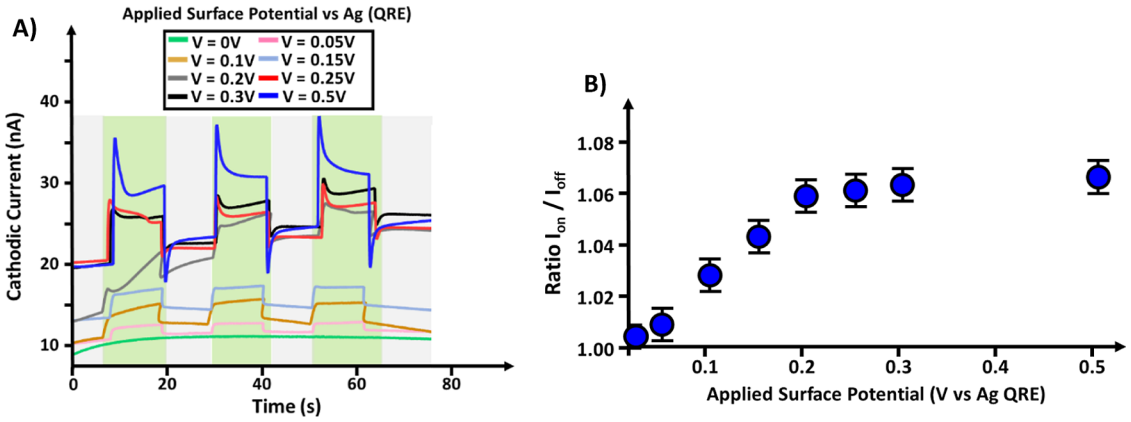

Figure 3. A) Electrochemical current vs time for steps at fixed tip potential (−0.9 V) and various substrate potentials indicated in the figure for the OFF (gray zones) and ON (green zones) states as defined in Figure 2. (B) Variation of the current contrast ratio as a function of the substrate potential. Tip−substrate distance = 10 μm.

with temperature in a nonlinear way[18] (this assumption will be tested further anyway). These results are the first indication that charge carrier injection should be the dominant process involved in the current enhancement. Moreover, when comparing the amount of tetrazine units converted during the plasmon activation (ca. 10 nC corresponding to 100 fmol) to the amount of photons injected during this period (650 μW leading to ca. 10^{16} photons with uncertainties due to losses), one can see that this latter is in large excess, making the electrochemical reaction feasible even if the photon to hole conversion has a very low yield. Finally, when looking at Figure 2B, one can notice the sharp increase of current upon plasmon activation, which is also a signature of charge carrier injection since thermal effects would lead to much slower processes.[20,32]

The average nanoparticle size on the plasmonic substrate was also varied in order to tune the matching between the excitation wavelength and the plasmon resonance while keeping the extinction constant at 650 nm (Figure 2A). The nanoparticle diameter can be tuned in a simple manner by changing the value of the electrodeposition potential. An example of particle size distribution obtained when electrodeposition is carried out at −1.1 V is shown in Figure S6. The results shown in Figure 2B,C confirm the expected behavior, namely, a gradual increase of the contrast ratio as the plasmon resonance wavelength gets closer to the laser excitation one (650 nm). The maximum value of r (1.13) is reached for the best matching. This value is comparable with the contrast ratio values obtained in a configuration where the gold nanoparticles were functionalized directly on the tip.[33]

In the next step, aiming to confirm and quantify that plasmon activation results mainly in hole injection in the solution, another control experiment was performed: SECM was now employed in feedback mode with substrate polarization, i.e., in a 4-electrode configuration with two independent working electrodes, in the absence of plasmon activation. Figure 3 shows that polarizing the substrate at gradually more positive values has the same effect as the plasmon activation, that is, increasing the electrochemical current in the time interval where the potential is applied on the substrate. The maximal contrast ratio is obtained at a substrate potential of +0.3 V, which allows the reoxidation of the tetrazine anion radical to operate at the maximal rate. Similar values of the maximal contrast ratio (1.06) are measured in Figures 1−3, where the tip potential value is the same. Thus, it can be inferred that plasmon activation under these conditions (tip−substrate distance = 10 μm, irradiation power = 650 μW) leads to the same proportion of reductant and oxidant forms as the application of ca. + 0.3 V on the ITO substrate. Similar analyses can be obtained for other experimental conditions, enabling a quantitative comparison and an estimation of the equivalent redox potential of plasmon activation.

Fluorescence Response. The great advantage of performing such experiments with an electrofluorochromic probe is to dispose of two detection means: one electrochemical, based on the measured (tip or substrate) current, and one optical, based on the fluorescence intensity (and emission spectrum). This also allows direct imaging of the process in the region of interest (ROI) defined by a sphere extending between the tip and substrate (wide field detection) or closer to the substrate (confocal microscopy).

As fluorescence measurements involve excitation at 474 nm, a first control experiment was to check that this irradiation did not impact the electrochemical signal. Indeed, activation of interband electronic transitions is known to be also a source of charge injection in the surrounding medium.[34] Figure S7 shows that the electrochemical current measured at the tip is not modified by the 474 nm irradiation if the incident power density remains small. These conditions will be applied in the following.

A first picture of how plasmon activation affects the emitted light is given by the superimposition of the electrochemical signal, with the fluorescence images displayed in Figure 4. When the tip potential is put at −0.9 V (green zone), the electrochemical reduction of the probe induces a first fluorescence quenching that can be clearly seen in the images. This electrochemically induced quenching corresponds mainly to the conversion of emitting neutral tetrazines into their nonemitting anion radicals.[35] Upon plasmon activation, a deeper quenching is observed (zone 3 in Figure 4A), which is emphasized in Figure 4B (red zone) in the absence of electrochemical signal. The residual fluorescence needs the ROI to be shrunk to allow the detection, and Figure 4B shows that the intensity is reduced by ca. 10% upon plasmon activation.

To elucidate the origin of this additional quenching, a complementary set of experiments were conducted. The first one consisted of varying the tip potential from values where no

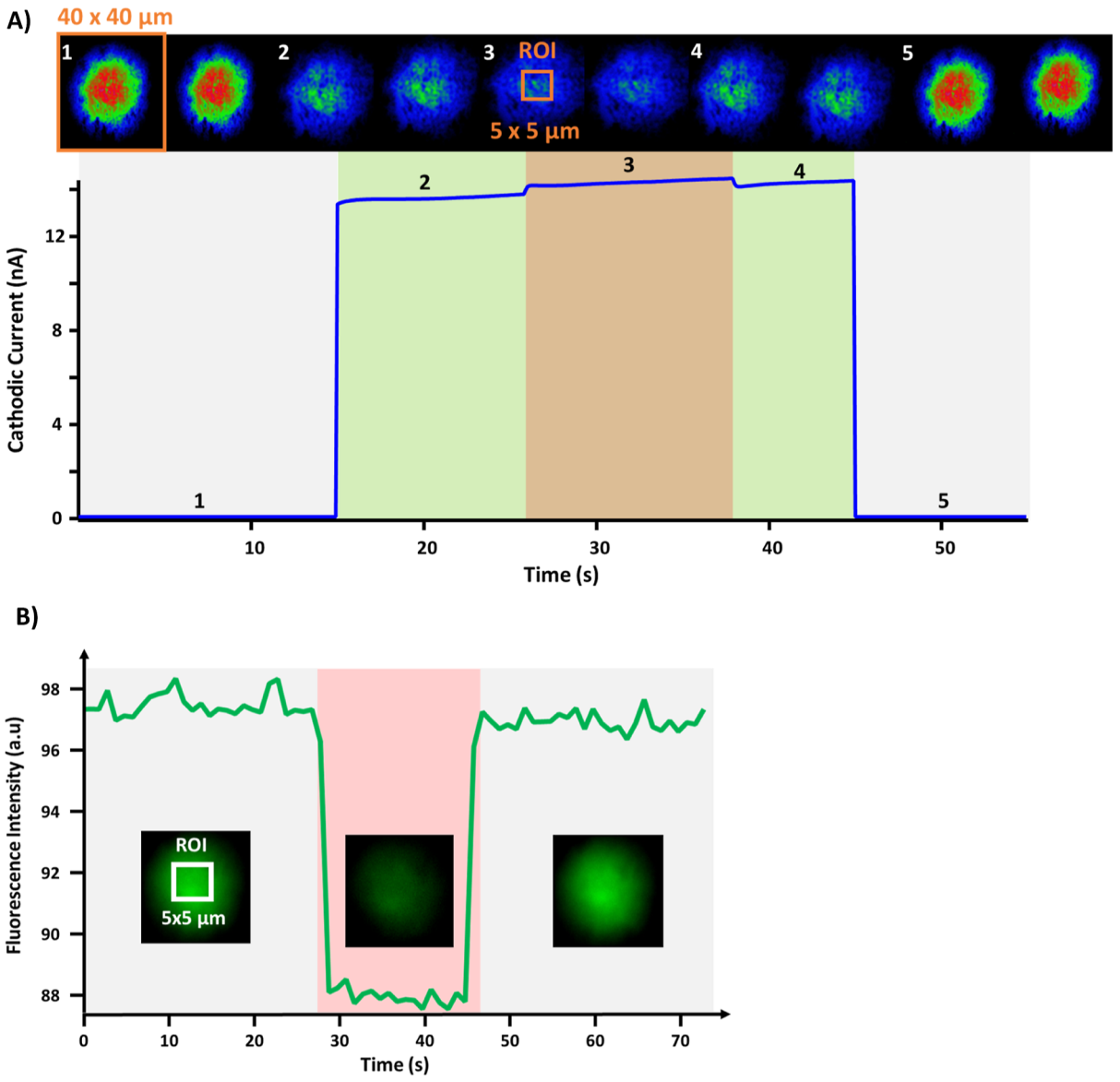

Figure 4. A) Fluorescence images of the region of interest (ROI) and electrochemical currents vs time corresponding to the tip potential varying from 0 V (gray zone) to −0.9 V (green and brown zones). 1 = Start of the excitation (470 nm) and fluorescence recording. 2 = Start of the electrochemical activation; and 3 = Start of plasmonic activation (red laser 650 nm, 650 μW). (B) Fluorescence intensity at 536 ± 20 nm (excitation wavelength = 470 nm) and images of a ROI (5 × 5 μm) vs time in the absence (gray) and presence (red) of plasmonic activation (red laser 650 nm, 650 μW) in the absence of electrochemical signal.

electrochemical reaction occurs until values where the electrochemical conversion is complete. The results are displayed in Figure 5A. Two zones can be identified: the green one corresponding to the electrochemical quenching that starts to be observed when the tip potential is more negative than −0.4 V and the red one corresponding to the plasmon-induced quenching, which is observed whatever the tip potential but with different amplitudes according to its value.

To better quantify the impact of plasmon activation, we defined the relative quenching efficiency as

$$Q_{\text{eff}} = \frac{I_{\text{f(off)}} - I_{\text{f(on)}}}{I_{\text{f(off)}}}$$

where "off" and "on" indexes are related to the red laser state and I_f is the fluorescence intensity.

The variation of Q_{eff} with potential is shown in Figure 5B,C. Clearly, the quenching efficiency is larger as the tip potential is more positive, a variation that is the opposite of the electrochemical current ratio. When crossing these results with the electrochemical data (Figure 1), we can state that plasmon-induced charge injection is not observed at tip potentials more positive than −0.1 V. Thus, the observed fluorescence quenching upon plasmon activation, which can be seen in the high potential range can be assigned mostly to energy transfer between excited fluorophores and plasmonic nanoparticles, a phenomenon related to plasmon-enhanced Förster resonance energy transfer (PEFRET).[36] PEFRET is known to be strongly dependent on the spectral overlap between the energy donors and acceptors. In our case, the overlap integral is calculated from the emission spectrum of tetrazines (the energy donors) and the extinction spectrum of the energy acceptor (the gold nanoparticles). Based on this

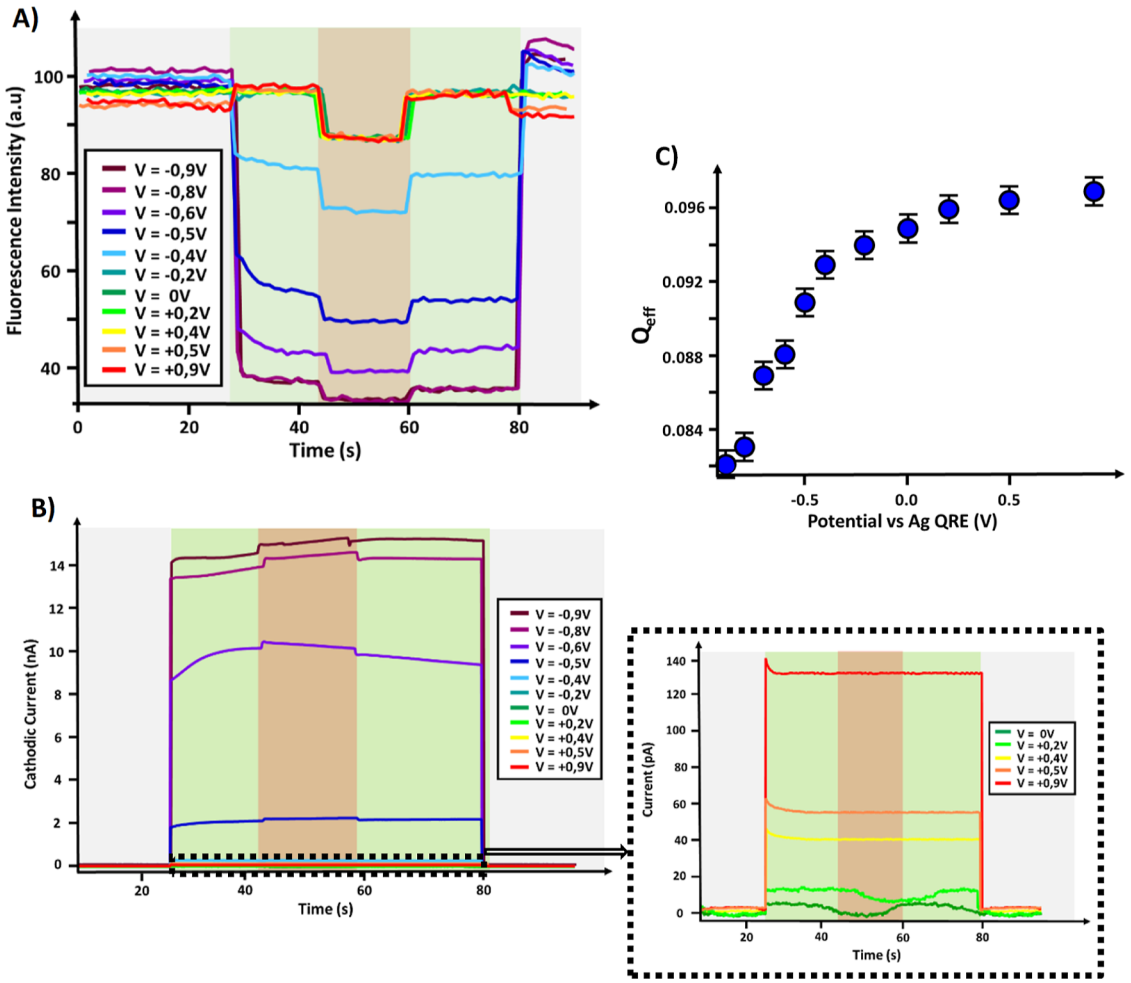

Figure 5. A) Fluorescence intensity at 536 ± 20 nm (excitation at 470 nm) vs time when the tip potential varies from 0 V to the indicated values (green zone). The brown zone corresponds to plasmon activation (red laser on, 4 kW cm^{-2}). (B) Corresponding tip current variations for the experiment in (A) (inset shows a magnification of the positive potentials range). (C) Fluorescence quenching efficiency corresponding to the brown zone of Figure 5A vs tip potential.

mechanism, energy transfer efficiency is expected to display a correlation with the normalized overlap integral J defined as follows:[14]

$$J = \frac{\int_0^\infty I_f(\lambda)\varepsilon(\lambda)\lambda^4 d\lambda}{\int_0^\infty I_f(\lambda)d\lambda}$$

where $I_f(\lambda)$ is the fluorescence intensity and $\varepsilon(\lambda)$ is the molar absorption coefficient[1] at wavelength λ.

Figure S8 shows the quenching efficiency measured for two plasmonic substrates having the same extinction at 650 nm but different plasmon bands. The one having the largest spectral overlap with the emission of the fluorophore gave the largest quenching (Table S1), supporting the proposed mechanism based on energy transfer. This results in the plasmon-induced fluorescence quenching observed in Figure 4B in the absence of electrochemistry. When an electrochemical current is induced between tip and substrate by applying a sufficiently negative potential at the tip, the plasmon-induced quenching becomes less efficient, which is consistent with the oxidation counter-reaction occurring at the substrate as it contributes to increase the fluorescence intensity. Of course, this process being restricted to the surface and the fluorescence detection being performed in a zone extending through the tip−substrate region, the overall intensity is not switched on again. Therefore, we decided to test the possibility to measure the fluorescence intensity closer to the surface through a confocal detection using a 100× objective with a higher NA. The results are displayed in Figure S9 and show the same trend as in Figure 5, but two main differences can be noticed. The first one is the larger Q_{eff} values in the high potential region in the absence of electrochemical reaction on the tip (Figure S9C). This relies on the better axial spatial resolution of the confocal technique with the fluorescence intensity being more sensitive to the nanoparticles. The field depth probed in this experiment can be estimated to 500 nm, thus much smaller than the tip−substrate distance. As the energy transfer process should be restricted to a few nanometers from the surface, it is likely that a strong interaction exists between the fluorophore and the gold nanoparticle surface; otherwise, the quenching efficiency would be much smaller. The second difference is the role of the tip potential, which leads to a larger drop in Q_{eff} in the confocal case. This is consistent with the higher sensitivity to the hole injection process, which contributes to increase the fluorescence intensity by reoxidizing the anion radicals into neutral emitting species, thus decreasing Q_{eff}.

In summary, the fluorescence results are consistent with the electrochemical results, with an additional quenching and a

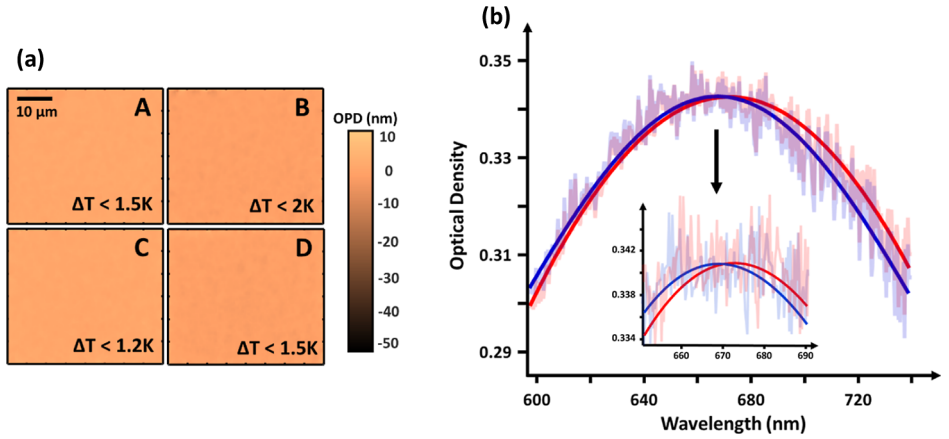

Figure 6. (a) Phase images (OPD = optical path difference) of gold nanoparticles during laser irradiation: on glass in acetonitrile (A), on glass in ethanol/acetonitrile mixture (90:10) (B), on ITO in acetonitrile (C), and on ITO in ethanol/acetonitrile mixture (90:10) (D). (b) Absorption spectra of gold nanoparticles before and after applying a 15 min chronoamperometry at −0.9 V vs Ag QRE to the SECM tip placed 10 μm above the substrate surface. Gaussian fits (χ^2 = 0.89) give λ_{max} = 673.7 ± 0.3 nm (red) and 668.5 ± 0.3 nm (blue) (see inset).

current enhancement upon plasmon activation. This is a major advantage of the combination of the two techniques using a single probe to disentangle processes involving charge transfer with direct consequence on the electrochemical response of those related to energy transfer and thus occurring in the absence of electrochemistry.

Investigation of Thermal Effects. Up to this point, charge carrier injection has been assumed to be the main mechanism involved in the plasmon-enhanced electrochemical current under our experimental conditions. Thermal effects are also to be considered when irradiating the plasmonic substrate with the red laser, but we have for the moment neglected their possible influence on the transport process of the redox probe. In order to support this assumption, we experimentally measured the local temperature profile in situ under irradiation.

Local thermal gradients can be conveniently measured using QPI,[37] particularly in the vicinity of plasmonic surfaces.[38−40] This family of techniques enables the measurement of thermally induced refractive index changes, therefore enabling indirect determination of the temperature profile.

To do that, a QPI module was added in the detection path of the fluorescence microscope, obtaining a configuration similar to the previously one used to monitor surface modification reactions.[37] We image the sample in transmission mode using a wide-field green light source (P = 500 mW cm^{-2}, λ_{obs} = 536 nm) to track any OPD arising from local solution heating without any risk of exciting the plasmons since we are off resonance. Subsequently, the experimentally measured OPD is used to determine the temperature difference with respect to a reference recorded with no plasmon excitation, according to eq 1

$$\mathrm{OPD} = \Delta n \times L_R = \frac{dn}{dT} \times \Delta T \times L_R \Rightarrow \Delta T = \frac{\mathrm{OPD}}{\frac{dn}{dT} \times L_R} \quad (1)$$

where n is the refractive index and L_R is the Rayleigh distance, which can be estimated from the beam radius ω_0 and wavelength λ as $L_R = \frac{\pi\omega_0^2}{\lambda}$. In the experimental conditions used for plasmon activation in our SECM studies (650 μW, i.e., ≈20 kW cm^{-2}), no OPD difference could be detected, meaning that the temperature increase, if any, falls below the noise level (∼1 nm) of the detection, as shown in Figure 6. To confirm that OPD is able to detect and measure temperature gradients, control experiments were conducted at higher laser power, where we deliberately heated the sample. With higher powers, temperature increases of several tens of degrees were measured with a good linearity for the temperature vs laser power relation (Figure S10). Based on the OPD noise levels and the calibration curve, we demonstrated that the maximal temperature elevation in the solution comprised between the tip and substrate was smaller than 2K. Such a small value insignificantly affects the solution transport phenomena and cannot account for the observed feedback current measured previously during red laser irradiation. Therefore, it is concluded that thermal effects have a negligible impact on transport phenomena in our system. This is notably related to the pulse excitation source that delivers a high amount of energy during the pulse itself (40 ps) but is allowed to relax during the waiting time before the next pulse (100 ns).

Evidence of Electron Accumulation. The previous results suggest that excitation of the plasmonic resonance of gold nanoparticles induces only a transfer of holes from the surface to the solution. The fate of the associated electrons produced upon plasmon excitation needs to be considered. A possible accumulation of electrons on the surface of gold nanoparticles may result from this process. Mulvaney et al.[41] demonstrated that the spectral band corresponding to plasmon resonance was blue-shifted as a consequence of accumulated negative charges on the nanoparticle surface. In order to perform a similar investigation, plasmonic substrates resonant at 650 nm were prepared on glass instead of ITO to prevent charge evacuation through the substrate. Subsequently, a potential step from 0 to −0.9 V vs Ag QRE was applied at the platinum tip positioned at 10 μm from the surface for 15 min in the presence of a tetrazine predegassed solution. Figure 6B compares the absorption spectra recorded before and after the chronoamperometry experiment and reveals evidence of electron accumulation. Indeed, a 5 nm blue shift is observed after plasmonic excitation combined with electrochemistry. Control experiments in the absence of plasmon activation (no red light irradiation) and in the absence of tip potential variation on the tip showed no variation of the plasmon resonance maximum (see Figure S11). Consequently, it can be

deduced that the nanoparticle surface gradually became negatively charged during chronoamperometry, confirming the previously postulated mechanism of hole transfer from metal to solution, while electrons remain on the nanoparticle surface. This situation was already reported for gold NPs with redox molecules adsorbed on it.[42] However, this conclusion only applies for glass substrate, and it is likely that ITO is sufficiently conductive to allow electrons to be evacuated from the place where they are produced.

CONCLUSIONS

We have demonstrated that plasmon activation triggered by exciting the plasmon resonance of gold nanoparticles on ITO in the presence of an electrolytic solution containing a redox fluorescent probe results in an oxidation process. This can be explained by a mechanism involving hole injection in the solution rather than electrons, despite the high electron affinity of the probe. A deep analysis, including several control experiments, shows that the maximal effect on the electrochemical current occurs when a perfect matching exists between the excitation wavelength and the plasmon resonance and a perfect alignment between the tip and the focal point of the excitation laser. A simultaneous measurement of the fluorescence intensity of the probe shows a double fluorescence quenching: an electrochemical and a plasmonic, the latter being assigned to an energy transfer between the fluorophore emission and the plasmon resonance of the gold nanoparticles, strongly dependent on the spectral overlap. Moving from wide-field to confocal microscopy enables to see the plasmonic quenching efficiency being larger in the absence of electrochemical reaction, consistently with the better sensitivity to the surface, but the drop when the applied potential becomes more negative is smaller, consistently with the hole injection process at the substrate surface. Additional experiments are, however, necessary to fully understand the quenching mechanism as the energy transfer range (a couple of nanometers from the surface) is unlikely to explain on its own the quenching efficiency values measured in both wide-field and confocal configurations.

From a practical point of view, this study demonstrates for the first time that electrofluorochromism, i.e., the reversible modulation of fluorescence according to the redox state, can be triggered by plasmons and detected in a dual optical and electrochemical manner. Further investigations are in progress to study similar effects with grafted molecules on the plasmonic substrate as it will allow us to get rid of the contribution of emitters far away from the plasmonic substrate surface, thus enhancing the detection sensitivity.

ASSOCIATED CONTENT

Supporting Information

The Supporting Information is available free of charge at https://pubs.acs.org/doi/10.1021/acs.jpcc.4c04648.

Data fitting procedures and additional figures (PDF)

AUTHOR INFORMATION

Corresponding Author

Fabien Miomandre − *Université Paris-Saclay, ENS Paris-Saclay, 91190 Gif Sur Yvette, France;* orcid.org/0000-0003-2001-9473; Email: mioman@ens-paris-saclay.fr

Authors

Ali Dabbous − *Université Paris-Saclay, ENS Paris-Saclay, 91190 Gif Sur Yvette, France*

Baptiste Maillot − *Université Paris-Saclay, ENS Paris-Saclay, 91190 Gif Sur Yvette, France*

Jean-Frédéric Audibert − *Université Paris-Saclay, ENS Paris-Saclay, 91190 Gif Sur Yvette, France*

Vitor Brasiliense − *Université Paris-Saclay, ENS Paris-Saclay, 91190 Gif Sur Yvette, France;* orcid.org/0000-0002-5515-2218

Complete contact information is available at: https://pubs.acs.org/10.1021/acs.jpcc.4c04648

Notes

The authors declare no competing financial interest.

ACKNOWLEDGMENTS

This work was funded by the French National Research Agency ANR APMJ (ANR 19-CE09-0013). Pr Alexa Courty and Dr Adrien Girard (Sorbonne U.) are warmly acknowledged for SEM-FEG experiments.

REFERENCES

(1) Nixon, R.; Contreras, E.; Jain, P. K. Electrochemistry with plasmons. *Trends Chem.* **2023**, *5* (8), 605−619.

(2) Zhan, C.; Chen, X.-J.; Yi, J.; Li, J.-F.; Wu, D.-Y.; Tian, Z.-Q. From plasmon-enhanced molecular spectroscopy to plasmon-mediated chemical reactions. *Nat. Rev. Chem* **2018**, *2* (9), 216−230.

(3) Qi, Y.; Brasiliense, V.; Ueltschi, T. W.; Park, J. E.; Wasielewski, M. R.; Schatz, G. C.; Van Duyne, R. P. Plasmon-Driven Chemistry in Ferri-/Ferrocyanide Gold Nanoparticle Oligomers: A SERS Study. *J. Am. Chem. Soc.* **2020**, *142* (30), 13120−13129.

(4) Choi, C. H.; Chung, K.; Nguyen, T. T. H.; Kim, D. H. Plasmon-Mediated Electrocatalysis for Sustainable Energy: From Electrochemical Conversion of Different Feedstocks to Fuel Cell Reactions. *ACS Energy Lett.* **2018**, *3* (6), 1415−1433.

(5) Ganguli, S.; Zhao, Z. W.; Parlak, O.; Hattori, Y.; Sa, J.; Sekretareva, A. Nano-Impact Single-Entity Electrochemistry Enables Plasmon-Enhanced Electrocatalysis. *Angew. Chem., Int. Ed.* **2023**, *62* (25), No. e202302394.

(6) Lee, J.; Mubeen, S.; Ji, X.; Stucky, G. D.; Moskovits, M. Plasmonic Photoanodes for Solar Water Splitting with Visible Light. *Nano Lett.* **2012**, *12* (9), 5014−5019.

(7) Zhang, Y.; Guo, W.; Zhang, Y.; Wei, W. D. Plasmonic Photoelectrochemistry: In View of Hot Carriers. *Adv. Mater.* **2021**, *33* (46), 2006654.

(8) Joshi, P. B.; Wilson, A. J. Plasmonically enhanced electrochemistry boosted by nonaqueous solvent. *J. Chem. Phys.* **2022**, *156*, 241101.

(9) Pang, L. Q.; Barras, A.; Mishyn, V.; Heyte, S.; Heuson, E.; Oubaha, H.; Sandu, G.; Melinte, S.; Boukherroub, R.; Szunerits, S. Plasmon-Driven Electrochemical Methanol Oxidation on Gold Nanohole Electrodes. *ACS Appl. Mater. Interfaces* **2020**, *12* (45), 50426−50432.

(10) Wei, Y.; Zhang, Y. C.; Pan, J. H.; Chen, T.; Xing, X.; Zhang, W. H.; Lu, Z. D. Plasmon-Enhanced Electrochemiluminescence at the Single-Nanoparticle Level. *Angew. Chem., Int. Ed.* **2023**, *135* (2), No. e202214103.

(11) Li, M. X.; Feng, Q. M.; Zhou, Z.; Zhao, W.; Xu, J. J.; Chen, H. Y. Plasmon-Enhanced Electrochemiluminescence for Nucleic Acid Detection Based on Gold Nanodendrites. *Anal. Chem.* **2018**, *90* (2), 1340−1347.

(12) Feng, X. Y.; Han, T.; Xiong, Y. F.; Wang, S. C.; Dai, T. Y.; Chen, J. H.; Zhang, X. J.; Wang, G. F. Plasmon-Enhanced Electrochemiluminescence of Silver Nanoclusters for microRNA Detection. *ACS Sens.* **2019**, *4* (6), 1633−1640.

(13) Dong, J.; Zhang, Z. L.; Zheng, H. R.; Sun, M. T. Recent Progress on Plasmon-Enhanced Fluorescence. *Nanophotonics* **2015**, *4* (4), 472−490.
(14) Lakowicz, J. R.; Ray, K.; Chowdhury, M.; Szmacinski, H.; Fu, Y.; Zhang, J.; Nowaczyk, K. Plasmon-controlled fluorescence: a new paradigm in fluorescence spectroscopy. *Analyst* **2008**, *133* (10), 1308−1346.
(15) Su, Q.; Jiang, C.; Gou, D. M.; Long, Y. Surface Plasmon-Assisted Fluorescence Enhancing and Quenching: From Theory to Application. *ACS Appl. Bio. Mater.* **2021**, *4* (6), 4684−4705.
(16) Audebert, P.; Miomandre, F. Electrofluorochromism: from molecular systems to set-up and display. *Chem. Sci.* **2013**, *4* (2), 575−584.
(17) Al-Kutubi, H.; Zafarani, H. R.; Rassaei, L.; Mathwig, K. Electrofluorochromic systems: Molecules and materials exhibiting redox-switchable fluorescence. *Eur. Polym. J.* **2016**, *83*, 478−498.
(18) Yu, Y.; Sundaresan, V.; Willets, K. A. Hot Carriers versus Thermal Effects: Resolving the Enhancement Mechanisms for Plasmon-Mediated Photoelectrochemical Reactions. *J. Phys. Chem. C* **2018**, *122* (9), 5040−5048.
(19) Zhan, C.; Liu, B.-W.; Huang, Y.-F.; Hu, S.; Ren, B.; Moskovits, M.; Tian, Z.-Q. Disentangling charge carrier from photothermal effects in plasmonic metal nanostructures. *Nat. Commun.* **2019**, *10* (1), 2671.
(20) Ou, W.; Zhou, B.; Shen, J.; Lo, T. W.; Lei, D.; Li, S.; Zhong, J.; Li, Y. Y.; Lu, J. Thermal and Nonthermal Effects in Plasmon-Mediated Electrochemistry at Nanostructured Ag Electrodes. *Angew. Chem., Int. Ed.* **2020**, *59* (17), 6790−6793.
(21) Guerret-Legras, L.; Audibert, J. F.; Dubacheva, G. V.; Miomandre, F. Combined scanning electrochemical and fluorescence microscopies using a tetrazine as a single redox and luminescent (electrofluorochromic) probe. *Chem. Sci.* **2018**, *9* (27), 5897−5905.
(22) Guerret-Legras, L.; Audibert, J. F.; Ojeda, I. G.; Dubacheva, G. V.; Miomandre, F. Combined SECM-fluorescence microscopy using a water-soluble electrofluorochromic dye as the redox mediator. *Electrochim. Acta* **2019**, *305*, 370−377.
(23) Liang, Z. R.; Li, J.; Zhou, Y. G. From Nanoparticle Ensembles to Single Nanoparticles: Techniques for the Investigation of Plasmon Enhanced Electrochemistry. *Chem.—Eur. J.* **2022**, *28* (53), No. e202201489.
(24) Yu, Y.; Williams, J. D.; Willets, K. A. Quantifying photothermal heating at plasmonic nanoparticles by scanning electrochemical microscopy. *Faraday Discuss.* **2018**, *210* (0), 29−39.
(25) Schorr, N. B.; Counihan, M. J.; Bhargava, R.; Rodríguez-López, J. Impact of Plasmonic Photothermal Effects on the Reactivity of Au Nanoparticle Modified Graphene Electrodes Visualized Using Scanning Electrochemical Microscopy. *Anal. Chem.* **2020**, *92* (5), 3666−3673.
(26) Miomandre, F. How molecular electrochemistry may shine light by designing electrofluorochromic compounds. *Curr. Opin. Electrochem.* **2020**, *24*, 56−62.
(27) Miomandre, F.; Audebert, P. 1,2,4,5-Tetrazines: An intriguing heterocycles family with outstanding characteristics in the field of luminescence and electrochemistry. *JJ. Photochem. Photobiol., C* **2020**, *44*, 100372.
(28) Oliveira de Miranda, L.; Maillot, B.; Bosmi, M.; Galmiche, L.; Audibert, J. F.; Decorse, P.; Brasiliense, V.; Berthelier, L.; Bonnamour, I.; Darbost, U.; Miomandre, F. Photophysical and Electrochemical Study of New Luminescent and Redox-Active Tetrazine Derivatives Grafted on Gold Nanoparticles. *J. Phys. Chem. C* **2023**, *127* (7), 3660−3670.
(29) Audebert, P.; Miomandre, F.; Clavier, G.; Vernieres, M. C.; Badre, S.; Meallet-Renault, R. Synthesis and properties of new tetrazines substituted by heteroatoms: Towards the world's smallest organic fluorophores. *Chem.—Eur. J.* **2005**, *11* (19), 5667−5673.
(30) Maillot, B.; Johnson, M.; Audibert, J. F.; Miomandre, F.; Brasiliense, V. *Operando* surface optical nanometrology reveals diazonium salts' visible photografting mechanism. *Nanoscale* **2023**, *15* (19), 8754−8761.
(31) Wu, T.; Guillon, M.; Gentner, C.; Rigneault, H.; Tessier, G.; Bon, P.; Berto, P. 3D nanoparticle superlocalization with a thin diffuser. *Opt. Lett.* **2022**, *47* (12), 3079−3082.
(32) Bagnall, A. J.; Ganguli, S.; Sekretareva, A. Hot or Not? Reassessing Mechanisms of Photocurrent Generation in Plasmon-Enhanced Electrocatalysis. *Angew. Chem., Int. Ed.* **2024**, *136* (7), No. e202314352.
(33) Zhou, Y.-L.; Zhang, P.-K.; Xu, C.-H.; Xu, J.-J.; Chen, H.-Y. An improvement in scanning electrochemical microscopy based on a plasmon-accelerated electrochemical reaction. *Chem. Commun.* **2019**, *55* (75), 11275−11278.
(34) Kamarudheen, R.; Aalbers, G. J. W.; Hamans, R. F.; Kamp, L. P. J.; Baldi, A. Distinguishing Among All Possible Activation Mechanisms of a Plasmon-Driven Chemical Reaction. *ACS Energy Lett.* **2020**, *5* (8), 2605−2613.
(35) Miomandre, F.; Lepicier, E.; Munteanu, S.; Galangau, O.; Audibert, J. F.; Meallet-Renault, R.; Audebert, P.; Pansu, R. B. Electrochemical Monitoring of the Fluorescence Emission of Tetrazine and Bodipy Dyes Using Total Internal Reflection Fluorescence Microscopy Coupled to Electrochemistry. *ACS Appl. Mater. Interfaces* **2011**, *3* (3), 690−696.
(36) Liu, H.; Li, C.; Li, J.; Cheng, Y.; Zhao, J.; Chen, J.; Sun, M. Plasmon-enhanced fluorescence resonance energy transfer in different nanostructures and nanomaterials. *Appl. Mater. Today* **2023**, *30*, 101731.
(37) Brasiliense, V.; Audibert, J. F.; Wu, T. F.; Tessier, G.; Berto, P.; Miomandre, F. Local Surface Chemistry Dynamically Monitored by Quantitative Phase Microscopy. *Small Methods* **2022**, *6*, 2100737.
(38) Baffou, G.; Bon, P.; Savatier, J.; Polleux, J.; Zhu, M.; Merlin, M.; Rigneault, H.; Monneret, S. Thermal Imaging of Nanostructures by Quantitative Optical Phase Analysis. *ACS Nano* **2012**, *6* (3), 2452−2458.
(39) Liu, C.; Tessier, G.; Flores Esparza, S. I.; Guillon, M.; Berto, P. Reconfigurable Temperature Control at the Microscale by Light Shaping. *ACS Photonics* **2019**, *6* (2), 422−428.
(40) Baffou, G.; Girard, C.; Quidant, R. Mapping Heat Origin in Plasmonic Structures. *Phys. Rev. Lett.* **2010**, *104* (13), 136805.
(41) Mulvaney, P. Surface Plasmon Spectroscopy of Nanosized Metal Particles. *Langmuir* **1996**, *12* (3), 788−800.
(42) Schlather, A. E.; Manjavacas, A.; Lauchner, A.; Marangoni, V. S.; DeSantis, C. J.; Nordlander, P.; Halas, N. J. Hot Hole Photoelectrochemistry on Au@SiO2@Au Nanoparticles. *J. Phys. Chem. Lett.* **2017**, *8* (9), 2060−2067.